



A Historical Earthquake-Induced Landslide Damming Event at the Qiaojia Reach of the Jinsha River, SE Tibetan Plateau: Implication for the Seismic Hazard of the Xiaojiang Fault

OPEN ACCESS

Mengmeng Hu^{1,2}, Zhonghai Wu^{1*}, Klaus Reicherter³, Sajid Ali^{3,4}, Xiaolong Huang¹ and Jiameng Zuo^{1,5}

Edited by:

Chong Xu,
Ministry of Emergency
Management, China

Reviewed by:

Ming Zhang,
China University of Geosciences
Wuhan, China

Xiangli He,
China Earthquake
Administration, China

Yulong Cui,
Anhui University of Science and
Technology, China

*Correspondence:

Zhonghai Wu
wuzhonghai8848@foxmail.com

Specialty section:

This article was submitted to
Geohazards and Georisks,
a section of the journal
Frontiers in Earth Science

Received: 05 January 2021

Accepted: 08 February 2021

Published: 16 March 2021

Citation:

Hu M, Wu Z, Reicherter K, Ali S,
Huang X and Zuo J (2021) A Historical
Earthquake-Induced Landslide
Damming Event at the Qiaojia Reach of
the Jinsha River, SE Tibetan Plateau:
Implication for the Seismic Hazard of
the Xiaojiang Fault.
Front. Earth Sci. 9:649543.
doi: 10.3389/feart.2021.649543

¹Key Laboratory of Neotectonic Movement and Geohazard, The Institute of Geomechanics, Chinese Academy of Geological Sciences, Beijing, China, ²School of Earth and Space Sciences, Peking University, Beijing, China, ³Neotectonics and Natural Hazards, RWTH Aachen University, Aachen, Germany, ⁴Department of Earth Sciences, COMSATS University Islamabad, Abbottabad Campus, Abbottabad, Pakistan, ⁵China University of Geosciences, Beijing, China

In bedrock mountainous areas where active faults and deep river valleys interact, earthquake-induced landslides can be used to explore local seismic hazards. The intersection of the highly active Xiaojiang Fault and the Jinsha River and its main tributaries in southwest China is a site of abundant earthquake-induced landslides. We found some boulders inappropriately scattered on the east bank of the Qiaojia reach of the Jinsha River, where the Qiaojia Segment of the Xiaojiang Fault passes through. We investigated the lithology and topography nearby and confirmed its source area, as well as the existence of a landslide damming event in the field. A high-resolution Digital Surface Model (DSM) generated from Unmanned Aerial Vehicle (UAV) images was used to analyze its characteristics and calculate its parameters. Optically Stimulated Luminescence (OSL) and ¹⁴C dating methods on the related dammed lake sand shows the age of the landslide, which is not later than 878 AD. The characteristics of large size with limited depositional extent, spatial relevance between the landslide and Xiaojiang Fault, and temporal-coincidence of the landslide with 624 AD earthquake support the seismic origin of this landslide. Moreover, the 624 AD earthquake was reanalyzed for its magnitude and macro-epicenter based on the coseismic displacement of the Heishui River floodplain. It was calculated to be Mw7.7 or Ms7.9 and relocated to the Qiaojia area. No M ≥ 7 earthquakes have occurred on the Qiaojia Segment for nearly 1,400 years since 624 AD. The elapsed time is close to the average recurrence interval of large earthquakes on the Qiaojia Segment. Therefore, the seismic hazard of the Qiaojia area should be considered in the future.

Keywords: Qiaojia, Jinsha River, earthquake-induced landslide, seismic hazard assessment, Xiaojiang Fault

INTRODUCTION

Landslides are a widely distributed geological process, commonly found in mountainous areas (Evans and Clague, 1994). Moreover, large landslides usually develop along rivers, giving rise to dammed lakes, which may eventually cause a subsequent catastrophic breach-flood. Based on morphology, displaced material type, mechanism of initiation, and other factors, landslides have been classified into many types (Bolt et al., 1977; Varnes, 1978; Highland and Bobrowsky, 2008), among which earthquakes can trigger every type. Landslides here are called earthquake-induced landslides. These landslides account for a large number of deaths and high economic losses, damaging engineering structures including settlements, dams, bridges, and communication systems (Keefer, 1984).

Earthquake-induced landslides can be used as indirect evidence to reconstruct the seismic history of a region without surface ruptures or environmental effects of earthquakes and should be implemented in hazard and risk studies (Jibson, 1996), which primarily focus on the likelihood, potential magnitude, and recurrence interval of large earthquakes in a region. Adams (1981) proposed that the magnitudes of prehistoric earthquakes could be estimated by comparing the extents of landslide dams of recent earthquakes with those of landslide dams in historical ones. Similarly, he has assessed the magnitude of the historical or prehistorical earthquake by comparing coseismic landslide distributions of prehistorical events with well-documented recent earthquakes in New Zealand and Central Asia (Adams, 1981). Practically, Zeng et al. (2020) used the empirical equations of the total volume of all paleolandslides triggered in an earthquake and the moment magnitude (Keefer, 1984) to evaluate the earthquake magnitude that triggered the Nixu rock avalanche event (~Mw7.0–7.2). Taking Soviet Central Asia as an example, Nikonov (1988) had an understanding: large seismo-gravitational dislocations, such as landslides, occur due to earthquakes of magnitude 6–6.5 or more and are always located within the highest isoseismal (about 10–25 km), tending to be along its major axis. Moreover, the number, size, and areal extent of the landslides are proportional to the size of an earthquake (Solonenko, 1977). Tibaldi et al. (1995) reconstructed the geometry of seismogenic faults by correlating the elongation of the landslide distribution with the location and dimensions of the faults. According to a statistical analysis of 40 historical worldwide earthquakes, the relationship between landslide distribution and seismic parameters was analyzed (Keefer, 1984). Later, the upper bound of the maximum distance to landslides from the epicenter and fault rupture zone for earthquakes of different magnitudes was determined (Jibson, 1996; Jibson, 2009; McCalpin, 2009). Meunier et al. (2007) derived an expression for the spatial variation of landslide density analogous with regional seismic attenuation laws, based on the observation on landsliding associated with large earthquakes on three thrust faults: the Northridge earthquake in California, Chi-Chi earthquake in Taiwan, and two earthquakes on the Ramu-Markham fault. Massey et al. (2018) investigated the landslides accompanying with the 2014 November 2016

Mw7.8 Kaikōura earthquake, and found: 1) seven of the largest eight landslides (from 5 to 20 Mm³) occurred on faults that ruptured to the surface during the earthquake; 2) the average landslide density within 200 m of a mapped surface fault rupture is three times than that at a distance of 2,500 m or more from a mapped surface fault rupture.

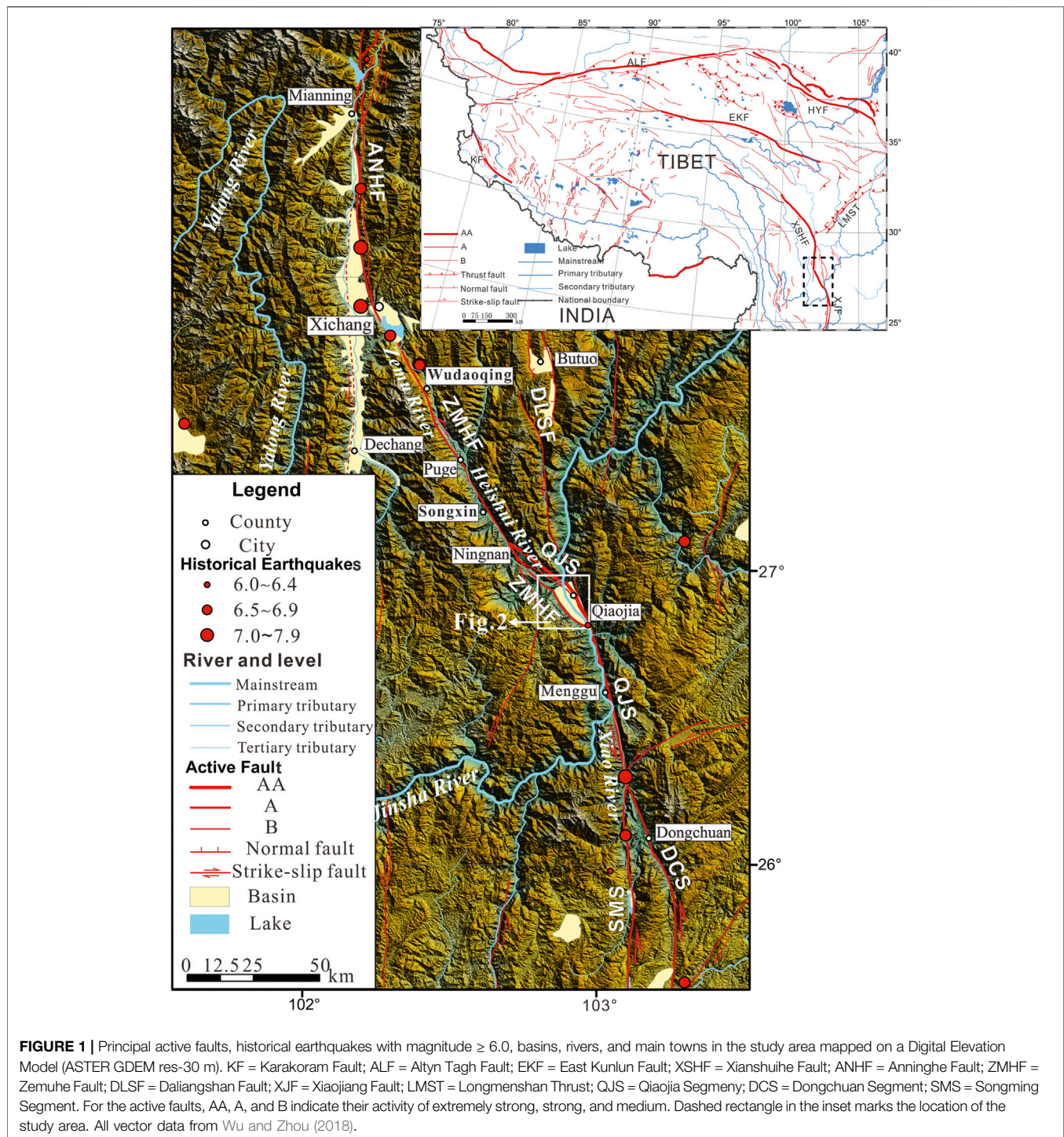
The SE Tibetan Plateau, located between the Eastern Himalayan Syntaxis and the Sichuan Basin, contains numerous active faults, large relief, and a well-developed river network. Three major rivers, the Jinsha, the Lancang, and the Nu, flow from NW to SSE in parallel (Liu et al., 2009). A series of landslide blocking events were found along the rivers previously. Using the Interferometric synthetic aperture radar (InSAR) method, 22 active landslides were identified and mapped over more than 2,500 km² in the reservoir of the Wudongde hydropower station, Jinsha River (Zhao et al., 2018). The ancient Zhaizicun landslide blocked the Jinsha River, and the lacustrine sediments developed upstream of the landslide dam (Xu et al., 2011; Zhang et al., 2012). The Chongjianghe landslide, a giant landslide discovered by Zhang et al. (2013) in the Chongjianghe Screw Bay Power Station, a branch of the Jinsha River in northwestern Yunnan, is located in the step over of a regional active fault.

We found some boulders inappropriately scattered on the east bank of the Qiaojia reach of the Jinsha River in the field, where the Qiaojia Segment of the Xiaojiang Fault passes through. Lithology and surrounding topography indicate its source location, implying a landslide damming event occurred before. A high-resolution DSM generated from UAV images was used to analyze the characteristics and calculate the parameters of this landslide. Simultaneously, OSL and ¹⁴C dating methods were used to determine its age. Moreover, we attempted to demonstrate its seismic origin mechanism. Combined with the analysis of a coseismic displacement on the Qiaojia Segment near this landslide, we discussed the seismic hazard of the Qiaojia Segment.

REGIONAL SETTINGS

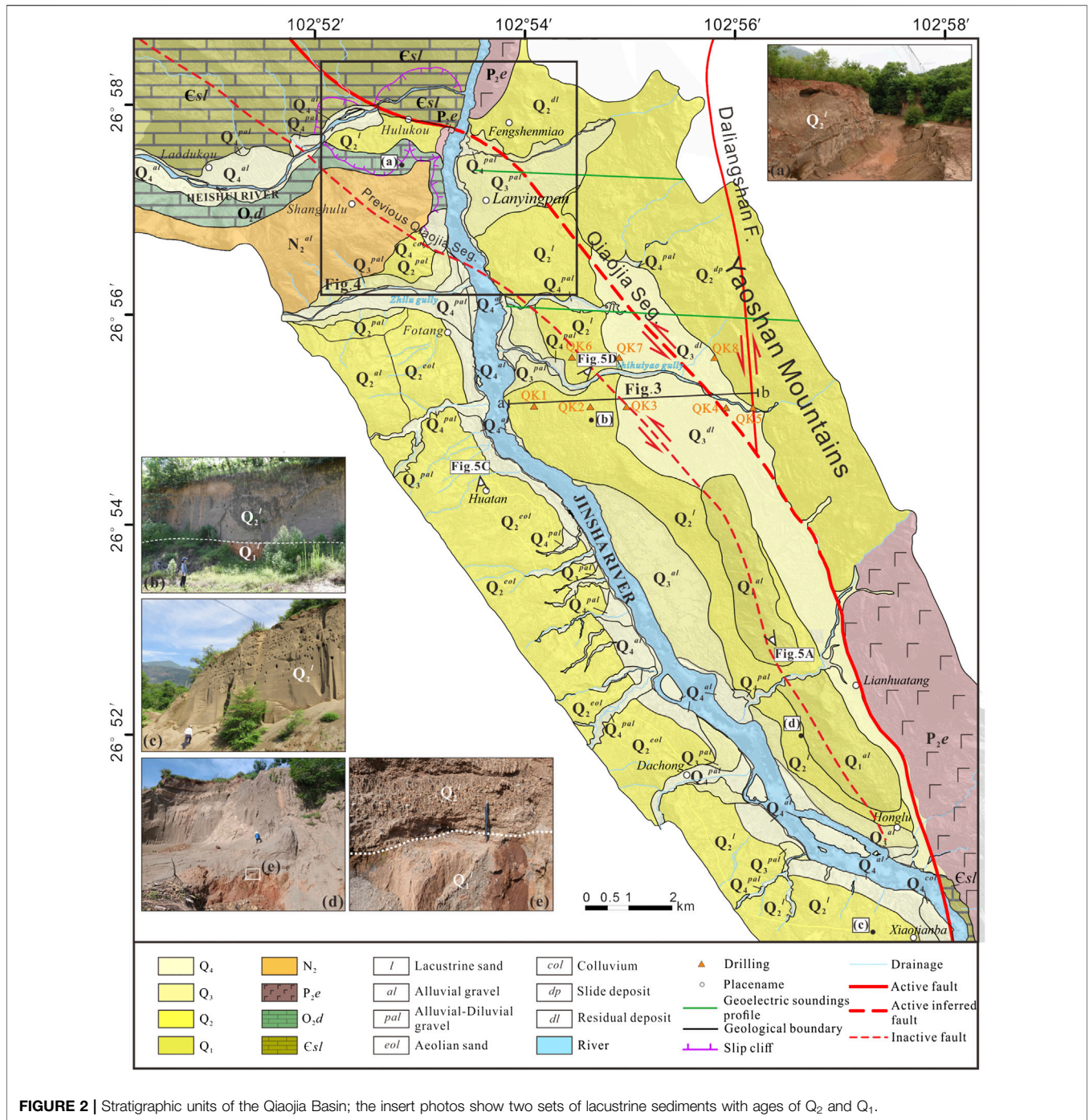
Geography

At the Qiaojia reach of the Jinsha River, the curve traces of three major active faults (the northern segment of the Xiaojiang Fault (Qiaojia Segment), Zemuhe Fault, and Daliangshan Fault) intersect, forming the Qiaojia Pull-Apart Basin (Figure 1). The Yaoshan Mountains and the Jinsha River, to the east and the west respectively, bound the Qiaojia Basin, while Hulukou and Xiaotianba restrict it in the north and south (Figure 2). The overall shape of the basin is a 15 km long and 4 km wide narrow wedge, having an N-S orientation and an average slope of about 7°. Significantly, the north-flowing Jinsha River conferred a ladder terrain, including three terraces and a flood platform. These terraces lie between 640 and 750 m elevation and the flood platform exists between 750 and 1,000 m elevation from the back-end of the terrace to the foot of the Yaoshan Mountains (Figure 3). In addition, some incised valleys and terraces developed across the platform. The west side of the Jinsha River is divided by the Zhilu Gully, having the Wushenggong



Ridge (up to an elevation of 1,060 m) to its north and the Low Mountain, hilly landform with medium fluctuation to its south. Close to the boulders, the topography of both sides of the Jinsha River is significantly different (**Figure 4**). On the east side, a Q_3 proluvial-alluvial fan originates from a mountain pass, with a low slope angle (4.6°), spreading at least 2 km from the east bank to the mountain foot. On the west side, the valley shoulder (elevation 870 m, and 240 m above the river surface) of the

Wushengong Ridge separates the gently sloping terrain above it from the alternate terrain of the abrupt wall and the narrow gentle slope below it. The comprehensive terrain slope under the valley shoulder is about 42° . Separated from the Wushengong Ridge by a gully, the accumulative hill is 760 m high at most, occupying an area of 0.13 km^2 . Moreover, the limestone bedrock hill between Hulukou Town and the Heishui River locates at the site where the width of the Jinsha River abruptly narrows from



200 to 120 m. Its top elevation is 866 m. The Qiaojia Segment traces on its south side, forming a fault scarp.

The climate in the dry-hot valley of the Jinsha River is arid, and the water and heat are extremely unbalanced. Located in the river valley, Qiaojia Basin has an annual average temperature of more than 20°C. The average temperature of the hottest month, July, is 27.4°C, and the average temperature of the coldest month, January, is 12.2°C. According to the data of major climate stations in the Qiaojia area, the annual precipitation varies

from 600 to 1,600 mm from Jinsha River Valley to the mountains above 3,000 m.

Geology

The Qiaojia Basin is mainly controlled by the Qiaojia Segment (Figure 2). About 80 km long, the Qiaojia Segment extends nearly N-S with an almost upright dip angle from Daduo in the south and north of Qiaojia in the north. The trace and location of this segment in the Qiaojia Basin can only be identified from the offset

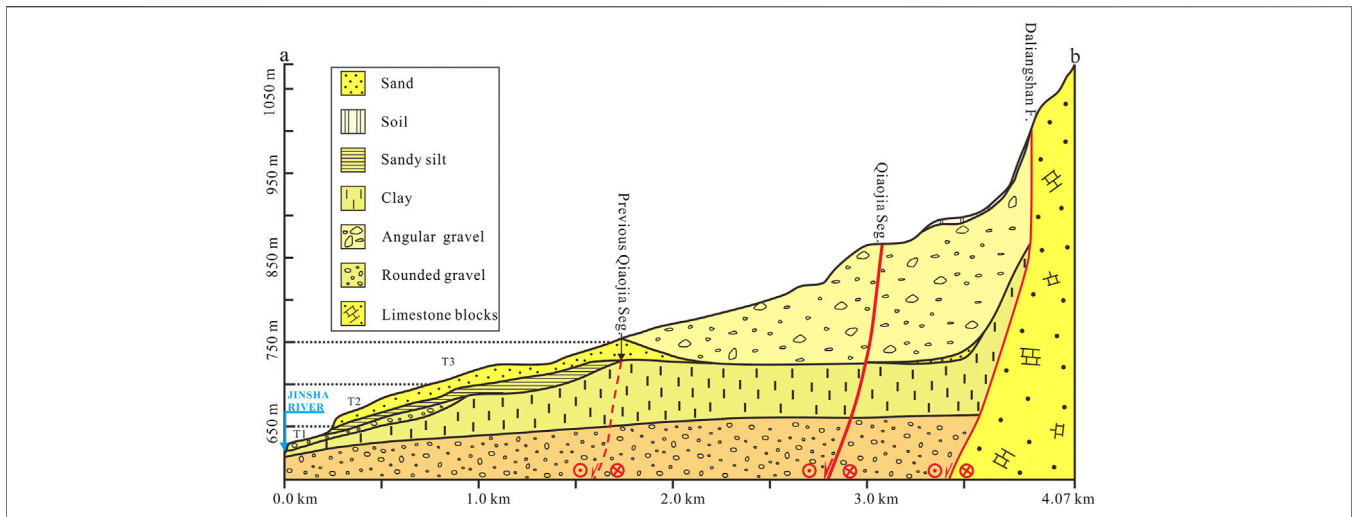


FIGURE 3 | Cross-section of Qiaojia Basin, showing the three terraces of the Jinsha River and a flood platform behind them; from the drill data of Li et al. (2016); see the location of the drills in **Figure 1**.



FIGURE 4 | DSM (res-0.6 m) of the topography around the landslide; red solid line and thick red dashed line indicate the current Qiaojia Segment trace, thin red dashed line indicates the previous Qiaojia Segment trace; jagged white lines show the crown of the early landslides; yellow solid lines circle the source of the failed slope collapse to be discussed in this paper, yellow dashed lines to the west of the Jinsha River indicate the near-source deposit, and the yellow dashed line to the east of the Jinsha River circles the spatial distribution of boulders from this failed slope collapse. All terraces are outlined with black lines. Solid orange rectangle shows the sample locations, as well as the locations in **Figure 9**.

of several stream channels and the geoelectric soundings at overlying thick Quaternary sediment sites. It changes trend from nearly N-S to a NW direction, crossing the basin and

connecting to the Zemuhe Fault near Ningnan. The strike-slip rate of the Qiaojia Segment was estimated at 7.0–10 mm/yr on a multiple-temporal scale from Late Quaternary to the modern

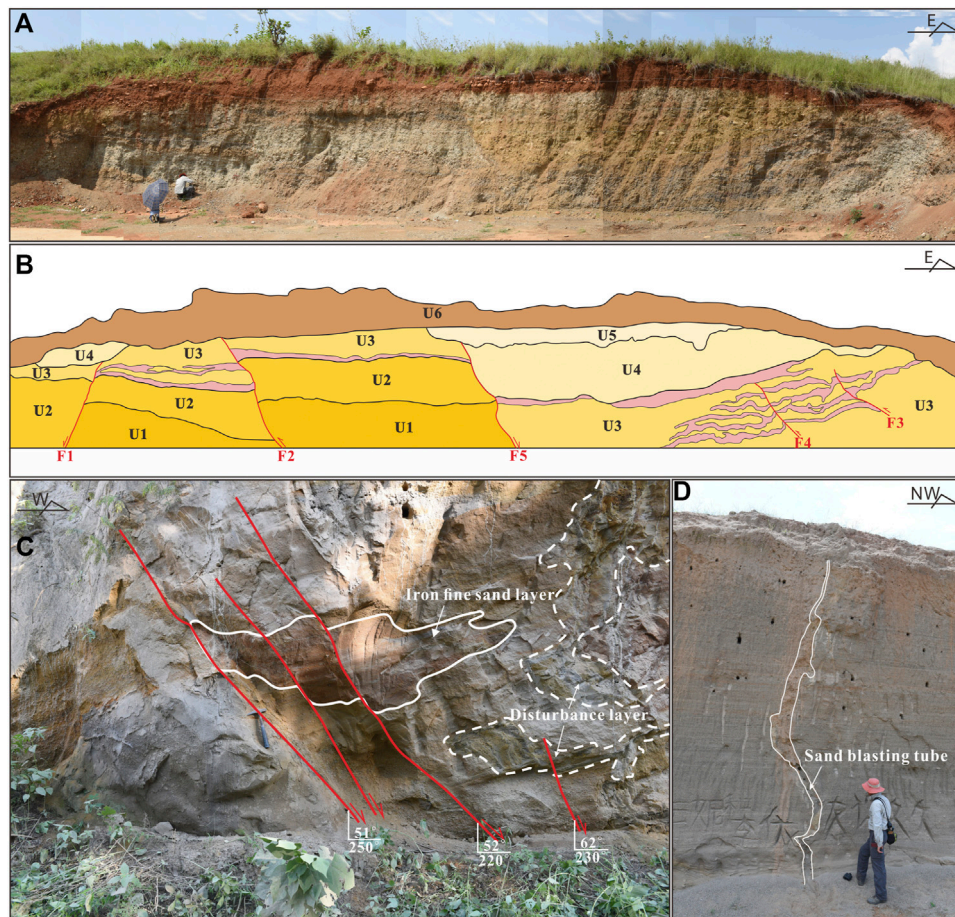


FIGURE 5 | Earthquake-induced effects in different sedimentary units (see the locations in **Figure 1**). **(A)** Small faults in Q_1^{al} ; **(B)** the interpretation of **(A)**, U1: gray gravel layer; U2: light grayish-green gravel layer; U3: inter-bedding of gray gravel layer and brown gray fine silty sand bearing gravel; U4: yellow-brown sand layer bearing gravel; U5: off-white calcareous consolidated gravel layer; U6: eolian brownish-red gravel layer (**lower**) and sand layer bearing gravel (**upper**); **(C)** Small faults and disturbance layer in Q_2^{al} brownish-yellow fluvial sand layer, the marker layer of a fault dislocation is an iron fine sand layer; the lime-green sand layer was disturbed; **(D)** sandblasting tube in Q_2^{al} medium-coarse lacustrine sand, the walls of the tube are calcareous cemented.

time (Wen et al., 2011; Wei et al., 2012; Zhao et al., 2015). Its previous trace was located to the west of the modern trace, proven to have ceased its activity by the latest dislocation strata dated to Q_2 .

Under the dual role of the north-flowing Jinsha River and the gullies from the eastern mountain, the Qiaojia Basin is characterized by a large amount of Quaternary fluvial sediments accumulated in the interior, including fluvial terraces, proluvial-alluvial fans, and lacustrine sediments. Among them, a large proportion of the lacustrine sediments are remarkable, with a wide exhibition range (**Figure 2**). Generally, we recognized two sets of lacustrine sediments linking to two large landslide damming events, referring to Q_1^l and Q_2^l according to the criterion of stratigraphic sedimentary sequence, which is constrained by strata of known age. These unconsolidated deposits are mainly sand and gravel and are more than 300 m thick. The Qiaojia Segment at Qiaojia Basin significantly fractured the bedrock on the west of the Jinsha

River, which would facilitate the occurrence of landslides. Accordingly, it has been observed that some landslides take place in some places downstream, damming the Jinsha River or its main tributaries (**Figure 4**).

Earthquakes

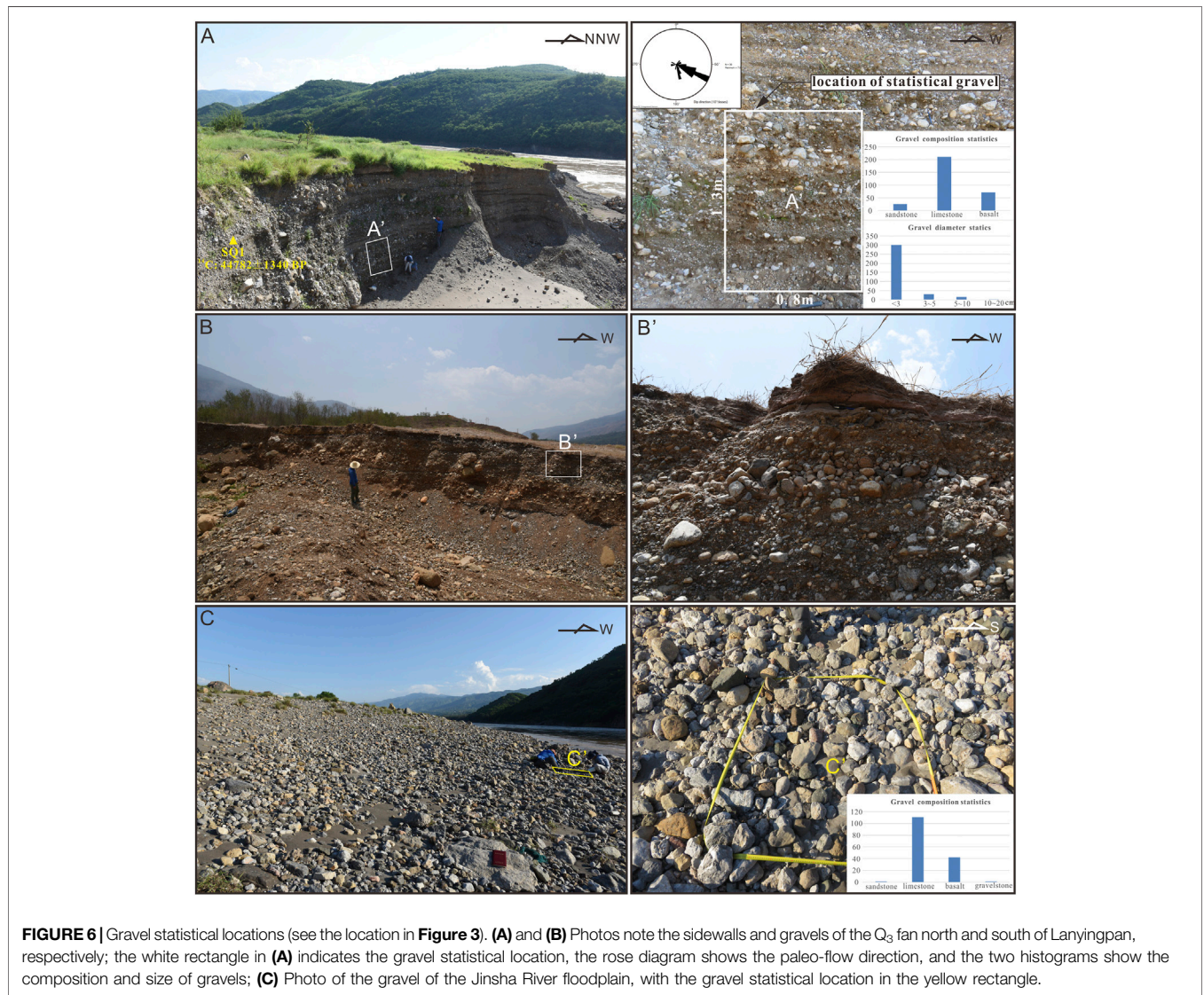
Seven historical earthquakes with magnitude ≥ 6.0 from Xichang to Dongchuan, mainly concentrated at the two end sites, with the maximum one occurred at Dongchuan in 1733 ($M 7^{3/4}$) (Department of Earthquake Damage Prevention, State Seismological Bureau, 1995) (**Figure 1**). The earthquakes recorded in the Qiaojia area were not as numerous as expected due to its special tectonic location. The historical earthquake catalog of the area indicates a seismic gap relative to the whole Xiaojiang Fault (Wen et al., 2011; Xu et al., 2017). Since 1500 AD, this area has been characterized by only one strong earthquake event (Qiaojia M_6 earthquake). Coseismic surface ruptures correspond to this earthquake distribution,

TABLE 1 | Results of OSL dating on the lacustrine sand.

Sample number	Material	Burial depth/m	Moisture content/%	Ambient dose rate/(Gy/ka)	Equivalent dose/Gy	Age/ka
SQ3	Medium-fine sand	0.1	6 ± 3	2.82 ± 0.08	5.02 ± 0.16	1.78 ± 0.07
SQ4	Medium-fine sand	0.35	8 ± 4	3.20 ± 0.10	5.65 ± 0.26	1.77 ± 0.10

TABLE 2 | Results of ¹⁴C dating.

Laboratory number	Sample code number	Material	Conventional radiocarbon age	2 sigma calendar calibrated results
Beta-509563	SQ1	Calcium film	43,310 ± 620 years BP	46,122–43,422 cal BC
Beta-509564	SQ2	Snail shell	1,110 ± 30 years BP	878–1,013 cal AD



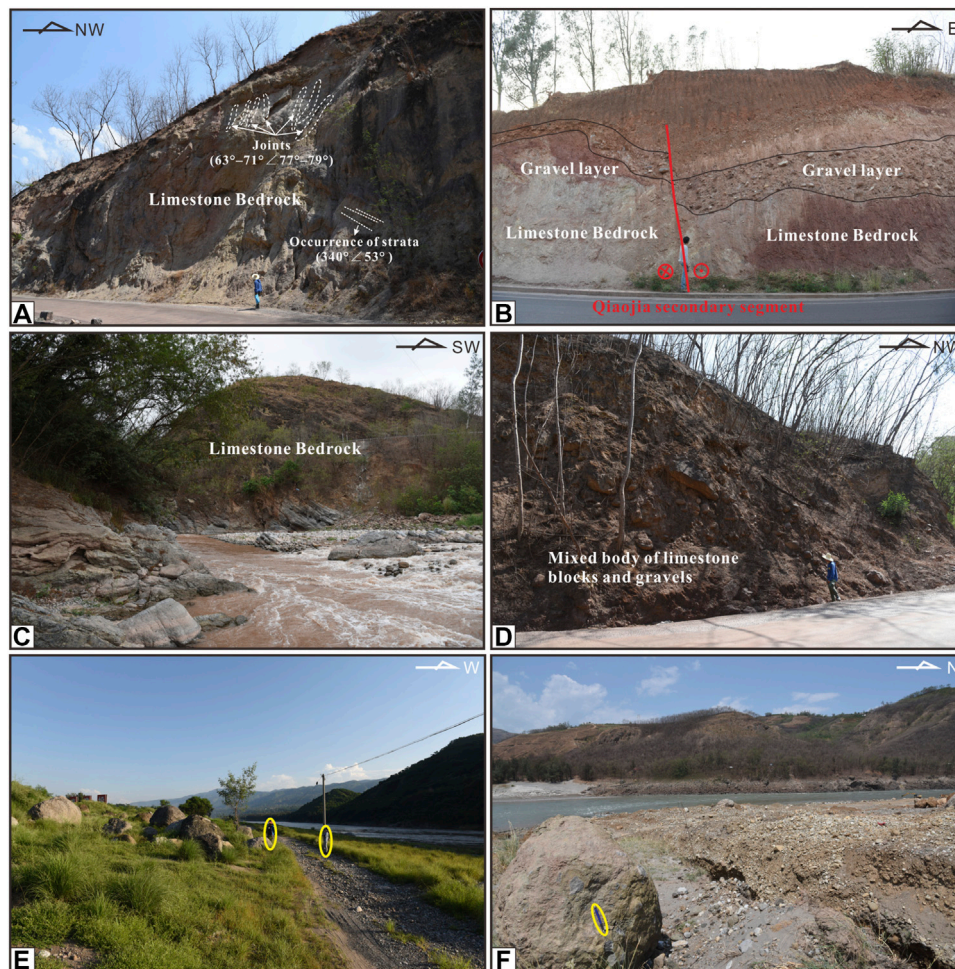


FIGURE 7 | Materials of the Wushengong Ridge and its adjacent hills. **(A)** limestone bedrock of the Wushengong Ridge; **(B)** terrace gravel layer overlying the limestone bedrock, in the Wushengong Ridge. The Qiaojia secondary segment can also be seen in this profile; **(C)** limestone bedrock of the hill north of Wushengong Ridge; **(D)** Mixed body of limestone boulders and gravels of the hill south of Wushengong Ridge. All locations are illustrated in **Figure 3**. **(E)**, **(F)** Field views of boulders at north and south of Lanyingpan, respectively, and person/pencil-outlined for scale. Locations in **Figure 7**.

which preserves a non-rupture section around the Qiaojia area (Wen et al., 2011). Paradoxically, a series of effects of earthquake-induced landslides are well preserved in the strata pre-Holocene, including small faults, disturbance layers, and sandblasting tubes (**Figure 5**), indicating the long-term earthquake silence in this area is abnormal.

DATA AND METHODS

Mapping the Landslide

In order to determine the characteristics and origin of this landslide, a combination of field investigation, satellite images from Google Earth, and a high-resolution DSM (res-0.6 m) generated with Structure from Motion (SfM) processing of UP30 Autopilot System photography were used. The SfM is an emerging and widely used photogrammetric method for reconstructing a 3-D structure using large sets of high-

resolution images with a high degree of overlap derived from a moving sensor (Snavely et al., 2008; Westoby et al., 2012; Lucieer et al., 2014). A detailed explanation of the SfM process is described in Snavely et al. (2008). Our collected images were processed using Agisoft Photoscan Pro software¹ with processing workflow procedures similar to that of Johnson et al. (2014). Hillshade was created in Global Mapper² from the high-resolution DSM and further processed in Coreldraw X7 for geomorphic mapping. To view and calculate the distribution and parameters of the landslide, we used the “Acute3D viewer” software³ to visualize the 3D demos generated from ContextCapture⁴.

¹www.agisoft.com

²https://www.blumarblegeo.com/

³https://acute3d-viewer.software.informer.com/

⁴https://www.bentley.com/en/products/brands/contextcapture

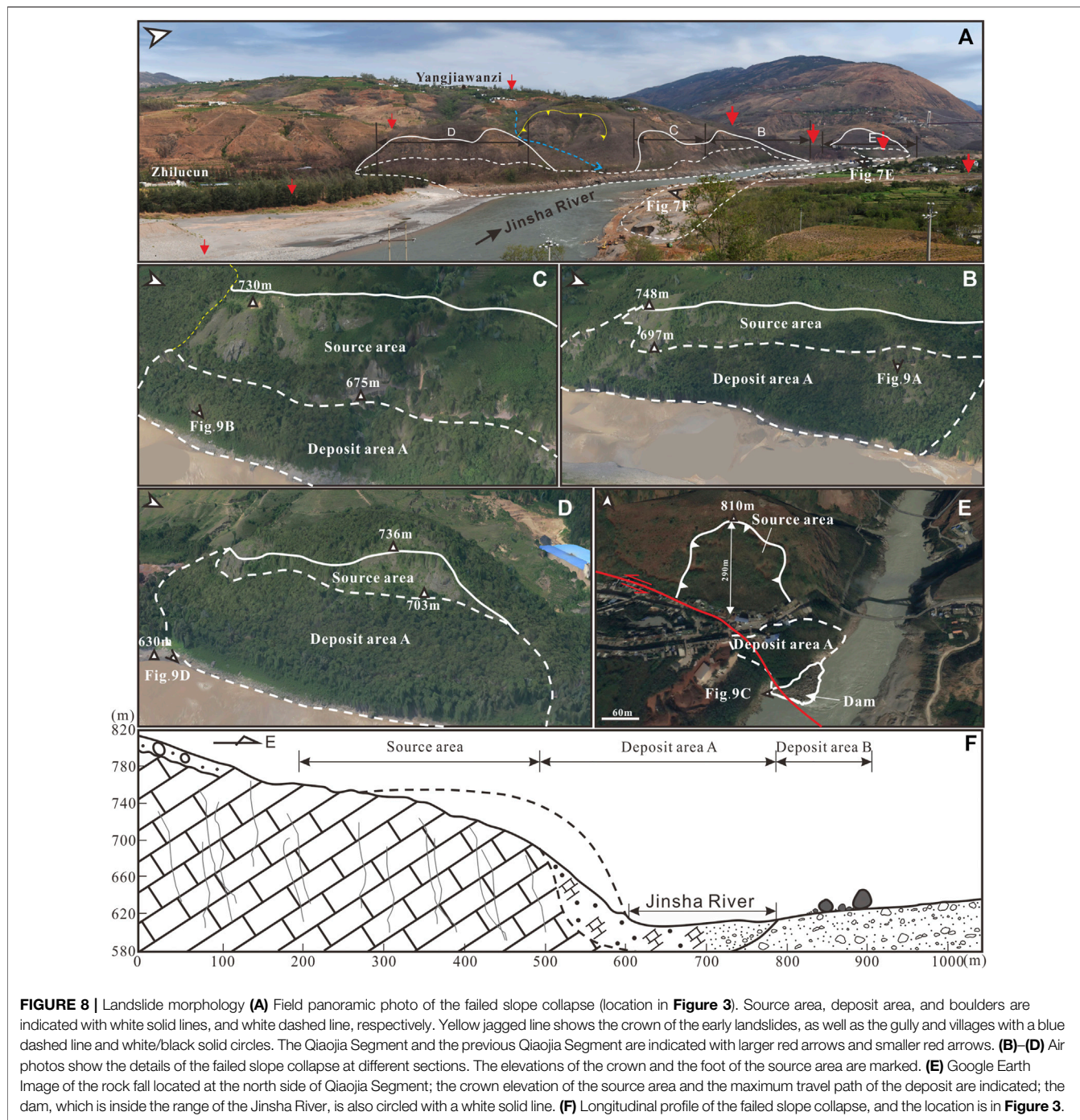


TABLE 3 | Characteristics of the failed slope collapse at different sections.

Section	Materials	Crown Elevation (m)	Drop (m)	Cut Volume (m ³)	Fill Volume (m ³)
B	Limestone bedrock	748	118	2,557,072.98	941,062.93
C	Limestone bedrock	730	100	1,326,247.92	118,034.27
D	Mixed body of limestone bedrock and gravels	736	106	717,513.26	627,118.52
E	Limestone bedrock	810	180	2,837,946.70	854,919.42

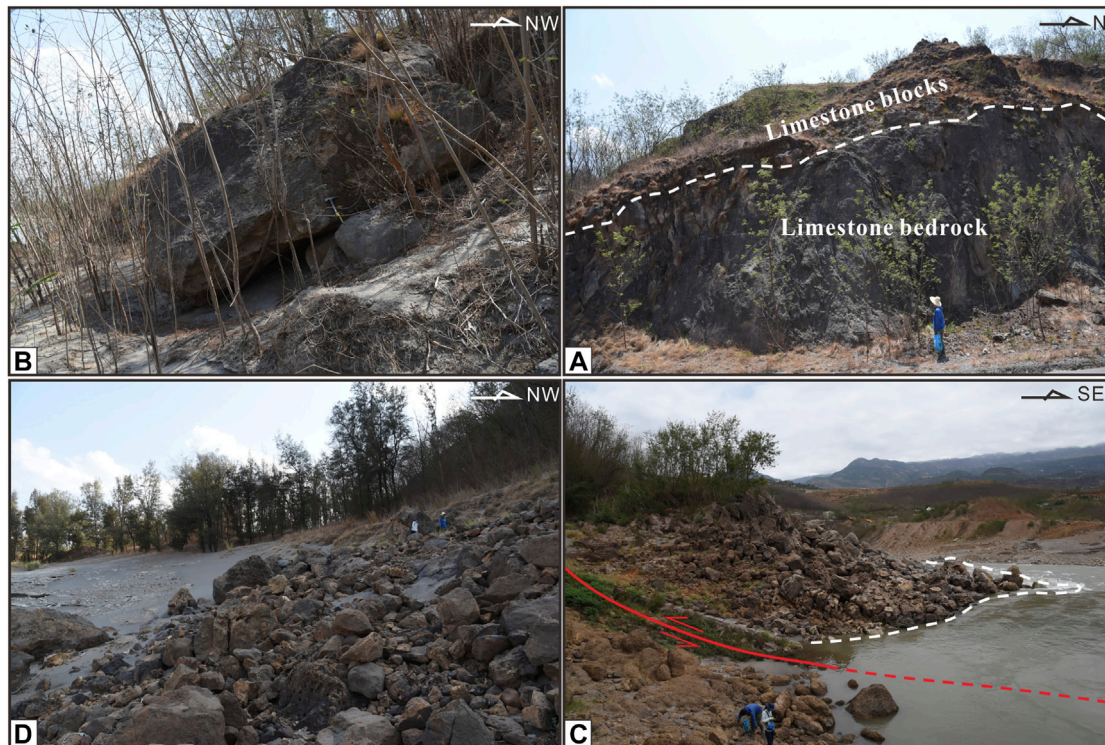


FIGURE 9 | (A) and (B) limestone boulders from the rock falls at sections (B) and (C); (C) Field view of the dam at the north side of Qiaojia Segment; (D) limestone boulders scatter on the west bank of the Jinsha River from the rock fall at section (D). All locations in **Figure 7**.

Dating

In this study, two OSL samples and two ^{14}C samples were dated. They are summarized in **Tables 1** and **2**, respectively.

The OSL samples were collected using stainless steel tubes (20 cm long and 5 cm diameter). The tubes were hammered into the sediment, and after completely filling, both ends were immediately sealed with aluminum foil and taped to prevent light leakage and loss of water during transport and storage. The sand can be easily sorted, and sizes of quartz particles in the range of 90–125 μm were chosen to date the sand. The whole dating process was carried out at the OSL/TL Geochronology Laboratory, Institute of Geology, China Seismological Bureau. Detailed processing and analytical procedures are reported in a previous study (Chen et al., 2013). The ^{14}C dating method used on the fossil snail shells buried in the sand precisely constrained the age of the sand. The sample was carried out at Beta Analytic Testing Laboratory, and the age was calibrated based on the INTCAL13 database on BetaCal3.21 software with 2σ (95% confidence limits). All the ages referred to hereafter in this paper are calendar years obtained from conventional radiocarbon ages.

RESULTS OF THE INVESTIGATION

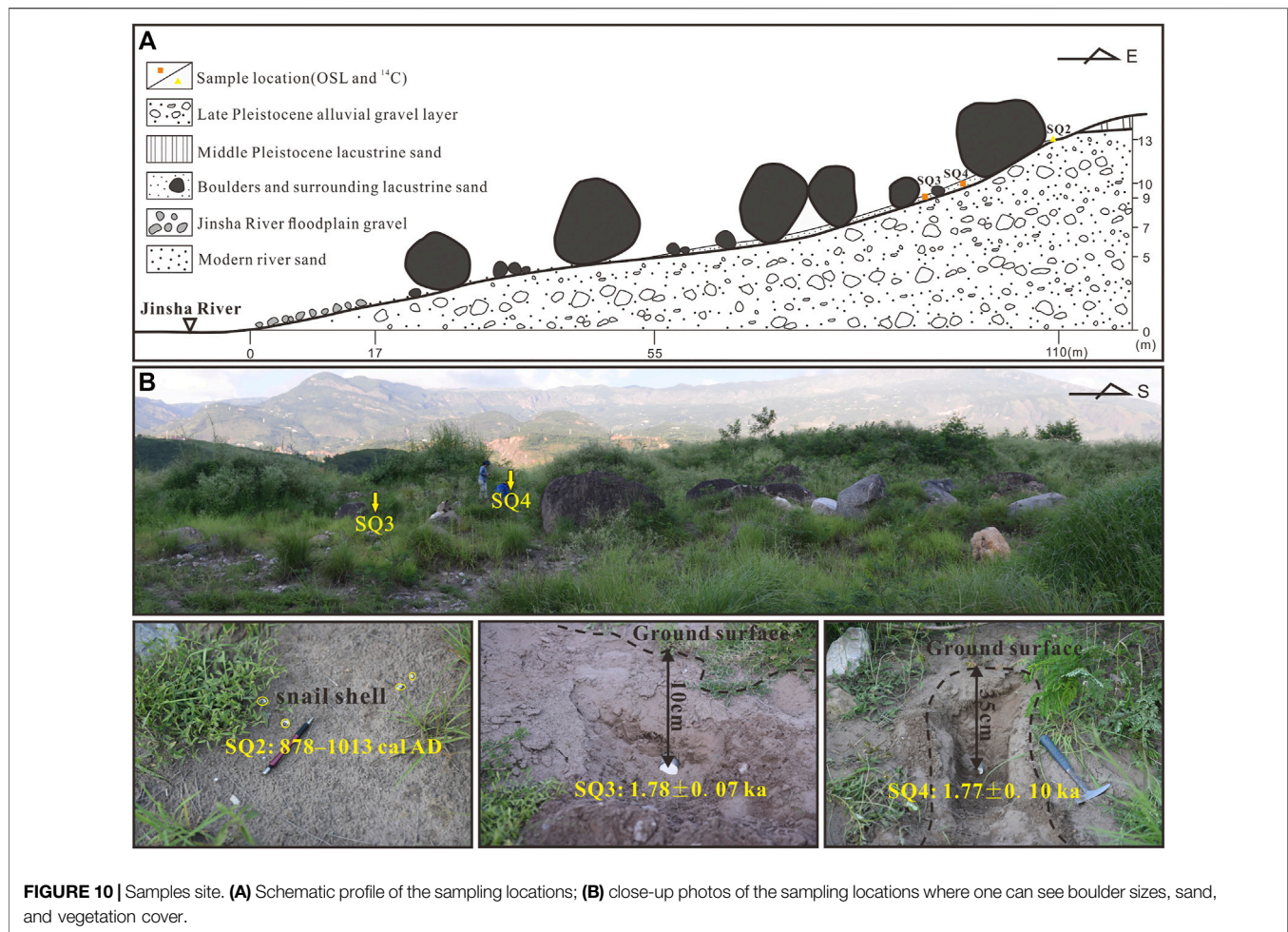
Existence of a Landslide

At the north of Lanyingpan, the fan underlying the boulders was dated to $44,782 \pm 1,340$ years BP using AMS- ^{14}C (Sample: SQ1,

Table 2). It is characterized by the inter-bedding of the coarse and fine gravel layers, with the gravel-bearing coarse sand lens occurring locally (**Figure 6A**). The gravel is mainly limestone, accounting for 85%–90%, with the remaining 10–15% being sandstone and basalt. The general flat-surface of the gravels inclines to the SEE, indicating it originated from the east mountain pass. The diameter of the gravels is predominantly several centimeters with few over 1 m. At the south of Lanyingpan, the gravels of the fan change in diameter to a smaller level, and the composition is also different from the above site, in which basalt is predominant, followed by limestone and sandstone (**Figure 6B**).

The gravels in the floodplain of the Jinsha River are mainly sub-angular and sub-circular in shape (**Figure 6C**). Their diameter is mainly 2–20 cm, followed by 20–30 cm, and a few 20–50 cm. In composition, limestone accounts for 70%, followed by basalt with 20–25%, and sandstone with 5–10%.

The Wushengong Ridge mainly consists of limestone bedrock, with sandstone and basalt developed locally, and a thick gravel layer overlain (**Figure 2**). The presence of the Qiaojia Segment has resulted in the limestone ($340^\circ \angle 53^\circ$) being intensely fragmented, having a set of steep joints ($63^\circ\text{--}71^\circ \angle 77^\circ\text{--}79^\circ$), which is consistent with the Qiaojia Segment on the strike (**Figure 7A**). The existing structures cause a reduction in the strength of the bedrock. Specifically, they may initiate small amounts of movement in a sliding mass and provide a path for potential water flow, which can cause



substantial engineering or construction difficulties, especially in the valley or canyon area (Bolt et al., 1977). The gravel layer is about 18–20 m thick and is characterized by alternating layers of coarse and fine gravel layers, where the gravel is dominantly extremely circular, with a maximum diameter above 50 cm and a primary composition of sandstone, spreading from an elevation of 770–1,060 m. It is cemented with calcareous material and forms a set of terrace gravel from the Heishui River (Figure 7B). The gravels are mainly sandstone with a diameter of 10–40 cm, which is consistent with the one on the Wushenggong Ridge. Moreover, the hill between Hulukou Town and the Heishui River is a limestone bedrock hill with the limestone extremely deformed (Figure 7C). The accumulative hill south of the Wushenggong Ridge is characterized by a mixed body of limestone boulders and sub-round but poorly sorted gravels, without underlying limestone bedrock (Figure 7D).

The boulders on the east bank of the river extend about 1.5 km long from north to south, centrally scattering at two sites. At the north of Lanyingpan, the boulders are even larger than a person (≤ 3.5 m) (Figure 7E). Limestone is their main composition, with a roundness of sub-angular to sub-circular. The farthest boulder

is 13 m above the river surface and is 100 and 287 m away from the east and west edges, respectively. At the south of Lanyingpan, the diameter of the boulders ranges from 0.8 to 1.4 m, with the same roundness and different compositions, mainly including limestone, followed by basalt breccia (Figure 7F).

Considering the coincidence of the composition and size between the boulders and materials of the Wushenggong Ridge and its adjacent hills, the source status of the ridge and its adjacent hills appear to be linked with the boulders. In addition, the steep topography on the west of Jinsha River, the spatial-correspondence between the boulders distribution and the range of the west slope, as well as the similar deposit on the foot of the west slope, all support the uniqueness of this origin. The Yaoshan Mountains east of Qiaojia Basin are exactly to land sliding, with several reports and research attesting to this (Wang, 1996; Feng et al., 2019). However, the ancient huge landslide occurred one hundred thousand years ago, and its stability has been proved. Over 10 m thick younger sediments overlay the frontal margin material of the landslide, as we introduced the stratum of Qiaojia Basin according to the field investigation and drill data. Thus, it is confirmed that a landslide originated from the Wushenggong Ridge and its adjacent hills.

TABLE 4 | Historical earthquakes before 878 AD in Xichang-Dongchuan area.

Date	Epicenter		Magnitude (Ms)	MMI	Description
	Latitude, longitude	References location			
624/08/15	27.9°, 102.2°	Xichang area	>6	VIII	Mountains shook, rivers were blocked with the dam
814/04/02	27.9°, 102.2°	Xichang area	7	IX	The aftershock lasted for 80 days, more than 100 people were crushed to death, and compression occurred within 15 km

Landslide Characteristics

The over 2 km long eastern flank of the Wushenggong Ridge, the accumulational hill south of it, and the bedrock hill north of it were observed as an entire failed slope (**Figure 8A**). It consists of several individual simultaneous landslides of different scales, crown elevations, materials, and slope angle (**Table 3**), complying with the criteria of a rock fall cluster (Keefer, 1984). The volumes of the total source area and the total deposit on the west bank are about 7×10^6 and 2.5×10^6 m³ respectively (extracted from the “Acute 3D Viewer” software). According to the classification of landslides on the basis of their magnitude (Parkash, 2012), this failed slope collapse was placed in an enormous category.

For the Wushenggong Ridge, two individual rock falls were focused (**Figures 8B,C**). At section C, fragment limestone blocks originated from an elevation of about 748 m, which is 118 m higher than the river surface (**Figure 8B**). The cut volume is far more than the fill volume, indicating a large amount of the materials transported into the river. The deposit on the west bank of the river is mainly composed of limestone boulders, with diameters ranging from 0.5 to 5 m (**Figures 9A,B**). The rock fall at section D shows similar features as the above one, with the crown elevation somewhat lower (730 m) (**Figure 8C**).

The materials of the accumulational hill failed with a wide range of collapse that occurred at a maximum elevation of 736 m (**Figure 8D**). The scattered limestone boulders (1–8 m diameter) on the west bank of the Jinsha River (**Figure 9D**) are products of the rock fall at this site.

At the south side of the limestone bedrock hill, Qiaojia Segment passes through, forming a fault scarp, which is prone to collapse. The limestone bedrock hill started to collapse at an elevation of 810 m. From crown to foot, the longest travel path of the rock masses is 290 m (**Figure 8E**). The accumulation of the limestone boulders (0.5–8 m diameter) stacked on the west bank of the Jinsha River is fresh without fillings, indicating the young age of the rock fall here. It even occupied half of the modern Jinsha River (**Figure 9C**) and was considered as a dam resulting in the dammed lake. With the boulders transported to the east bank of the Jinsha River, a dammed lake formed, and gray medium-fine sand spread around those boulders. This provides us an appropriate window to learn about the age limit of the landslide, which is almost equal to the age of the dammed lake sand.

Landslide Age

The 10–35 cm thick gray gravel-bearing medium-fine dammed lake sand layer begins to appear around the boulders 55 m away from the east edge of the river, spreading eastward to the end of

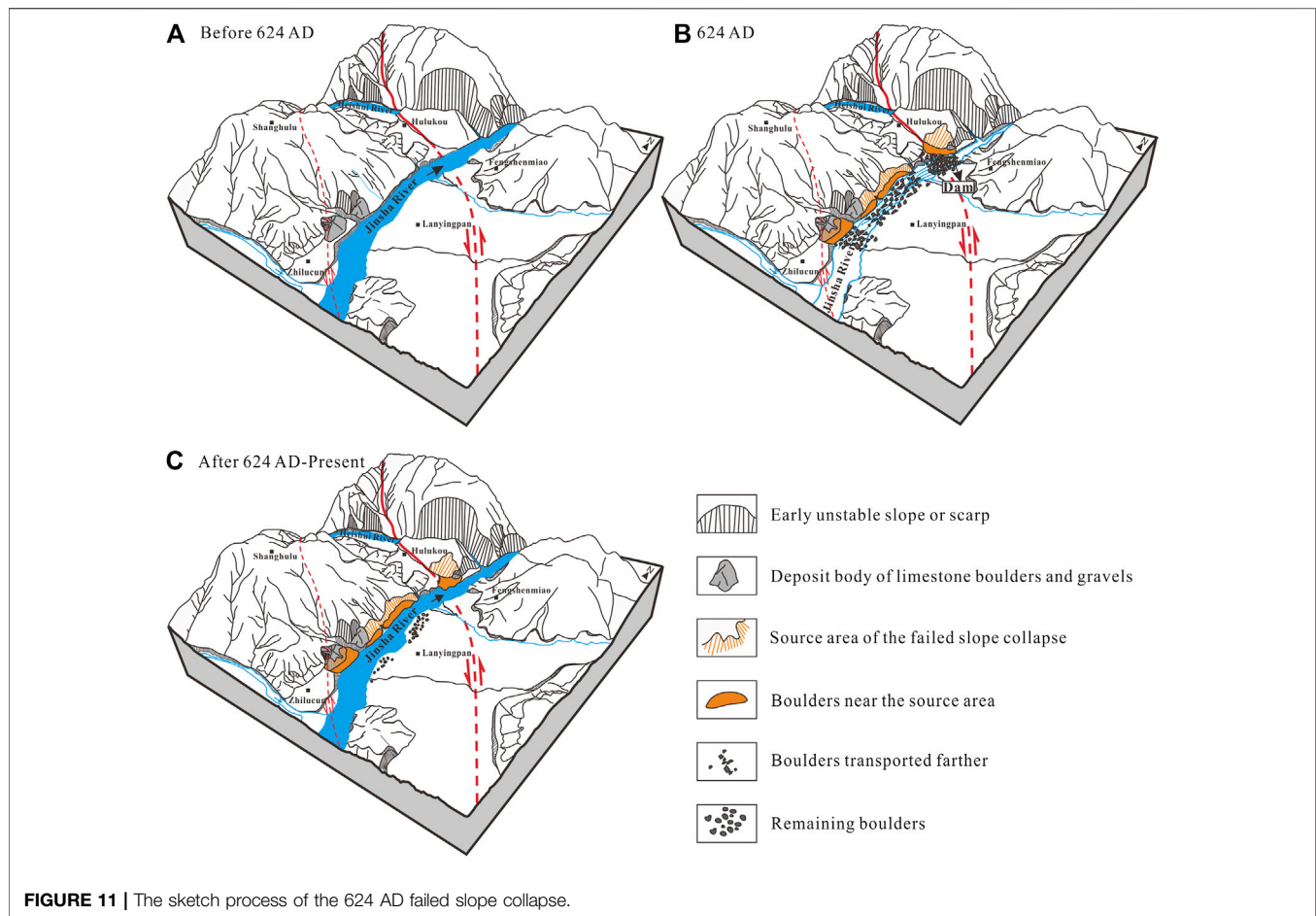
the boulders. We sampled with the profile perpendicular to the Jinsha River direction, where the boulders were exposed (**Figure 10**). The two dates from OSL samples (Samples: SQ3, SQ4) aged from 1770 to 1780 years BP (~240 AD) are older than the age of the ¹⁴C sample (Sample: SQ2, 878–1013 AD). According to the Timing principle of the OSL dating method, it determines the age of the last sunlight exposure event of the sample, thus more reliable result needs high degree of sunlight exposure and low residual OSL signals for the sample. However, as researched before (Zhang et al., 2015), when this method is applied with fluvial-lacustrine facies sand, the result could be used as a reference rather than accurate result, in the presence of other more reliable dating methods. In addition, the sand layer we sampled has experienced a rapid and transient sedimentary process, meaning an incomplete sunlight exposure. Thus, it is believed that the dammed lake formed before 878 AD.

DISCUSSION

Seismic Origin of the Landslide

A landslide occurs when the downslope component of the forces acting on the earth or rock mass exceeds the strength or shearing resistance of the material. The transition from a stable hillside to an active slide implies that either the acting force or the soil or rock resistance has changed for some reasons (Bolt et al., 1977). Several contributory causes were proposed, mostly including rainfall, earthquake, human activity, and so on (Cornforth, 2005). The annual precipitation of Qiaojia Basin is placed in the regionally low level and is the less rainy area. Considering the cluster characteristics of the landslide in a range of 2 km long, which cannot be realized with rainfall as a triggering factor, it is suggested that rainfall should be ruled out as a possible trigger of such a wide range of slope collapse. As a remote mountainous area, Qiaojia County is not a densely populated area historically, so human activity should also be excluded.

Uniqueness of the cause of landslide will be correlated with earthquake when some characteristics of the landslide possess. Spatial-relevance between landslides and active fault indicates that the landslides are seismically triggered (Burrows, 1975). Crozier (1992) proposes six criteria to support a seismic origin generally: 1) ongoing seismicity in the region, which has triggered landslides, 2) coincidence of landslide distribution with an active fault or seismic zone, 3) geotechnical slope-stability analyses showing that earthquake shaking would have been required to induce slope failure, 4) large size of landslides, 5) presence of liquefaction features associated with



landslides, and 6) landslide distribution that cannot be explained solely on the basis of geological or geomorphic conditions. Obviously, the more of these criteria that are satisfied, the stronger the case for seismic origin (Jibson, 1996). Keefer (1994) also mentions that in active seismic regions landslides with huge energy releases, large volumes and long runout distances have much higher probability of seismic origin than non-seismic origin. In addition, spatio-temporally correlating landslides with known or assumed earthquakes can increase the certainty of landslide seismic origin (Pánek, 2015). The landslide here meets several criteria of them.

Large Size With Limited Depositional Extent

A characteristic of the earthquake-induced landslide is its rapid occurrence, within a few minutes after the termination of the earthquake. The corresponding result of the rapid process of the landslide is its more limited depositional extent, which is different from that of the landslides that occur in intense rainfall conditions, characterized by more fluidity and a tendency to spread out farther across a depositional area (Perrin and Hancox, 1992). As mentioned above, this failed slope collapse is enormous in magnitude, with a characteristic of cluster. The boulders on the east bank distributed 1.5 km long in an N-S direction. We concluded that the general extent of the deposit did not

exceed the range of the source area (2 km long) transversely. The long horizontal distance against the small drop supports the effect of an earthquake. Further considering the blocky appearance of the deposits, we roughly confirm the seismic origin of this landslide.

Spatial Relevance Between the Landslide and Xiaojiang Active Fault

Zhang et al. (2018) recognized 94 landslides in the Qiaojia to Dongchuan area along the middle and northern segments of the Xiaojiang Fault based on GIS. The banded distribution of these landslides shows an obvious control by the fault, which corresponds with the surface rupture zone of strong earthquakes. Thus, it is believed that the Xiaojiang Fault controls the occurrence of landslides. Song et al. (2012) researched the deformation of the left bank of the Jinsha River around Baihetan Hydropower, about 40 km downstream of the Qiaojia Basin. He pointed out that the gently dipping faulted bedding belt and the NW trending fault are the main controlling factors of the deformation. For the left bank in the Qiaojia Basin, i.e., Wushenggong Ridge, a set of steep joints (63° – 71° \angle 77° – 79°) is consistent with the previous Qiaojia Segment on the strike. The small faults in the strata before the Holocene (**Figure 5A**) indicate

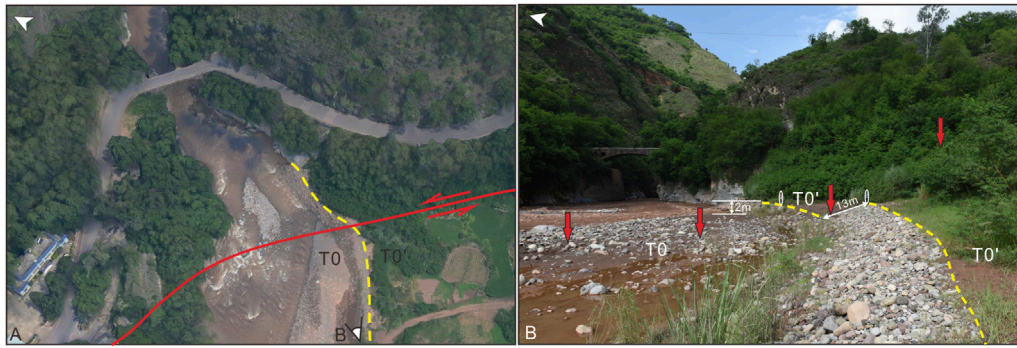


FIGURE 12 | (A) Air photo of the displacement of the Heishui River floodplain (see the location in **Figure 3**); **(B)** field view of the displacement of the Heishui River floodplain.

the existence of the non-active previous Qiaojia Segment, which is suggested to be the early location of the current Qiaojia Segment. The joints in the limestone of the Wushengong Ridge are located within the fault of the previous segment and present the rock fragmentation effect of its activity. Under such unstable slope conditions, the Wushengong Ridge is prone to collapse. After migrating to the Basin-Mountain margin east of Qiaojia County, the Qiaojia Segment has been acting in the extreme, having the potential to initiate earthquakes. As Jibson (2015) mentioned: landslides triggered in the immediate vicinity of active faults commonly are seismically triggered. The landslide in this paper straddles the Qiaojia Segment, indicating the possibility of being triggered by an earthquake event relevant to the activity of the fault.

Temporal-Coincidence of the Landslide With 624 AD Earthquake

Two earthquakes that occurred earlier than 878 AD in the study area are the 624 AD earthquake and the 814 AD earthquake (Lou, 1996). The former triggered landslides, resulting in river damming, whereas the latter was mainly characterized by ground compression (**Table 4**). Seismically induced permanent ground deformation is defined as any earthquake-generated process that leads to deformations within a soil medium, which, in turn, results in permanent horizontal or vertical displacements of the ground surface (Stewart and Wren, 2005). It includes the following modes: Surface fault rupture, liquefaction, seismically induced land sliding, and seismic compression. The requisite conditions for land sliding are the presence of sloping ground and the presence of combined static and dynamic shear stresses that exceed material strengths, whereas seismic compression needs relatively strong shaking and unsaturated soil of a flat site. These two modes correspond to the effects of the 624 AD earthquake and the 814 AD earthquake respectively, according to their descriptions. This means that the 814 AD earthquake probably occurred in a flat area such as Xichang Basin, while the 624 AD earthquake was more likely to have occurred in valley areas between Xichang and Qiaojia. And as mentioned before (Nikonov, 1988), large landslides, which are triggered by earthquakes of magnitude

6–6.5 or more, are always located within the highest isoseismal (about 10–25 km), tending to be along its major axis. Thereby, we confirmed the macro-epicenter of the 624 AD earthquake at somewhere of the Heishui valley, not far 25 km away from this landslide. Considering the remoteness of the ancient Xichang–Qiaojia area and the larger population in Xichang than in Qiaojia, it is understandable to arrange the Xichang as the macro-epicenter of the 624 AD earthquake in the historical catalog. The description of the 624 AD earthquake and its spatial proximity to the studied landslide support its greater plausibility as the trigger of this landslide than the 814 AD earthquake.

Accordingly, the seismic origin of this landslide is basically determined, termed as a coseismic event of the 624 AD earthquake.

Process of the Landslide

Long-term activities of the Qiaojia Segment have led to the fragmentation of rock masses on both sides of the fault. Weakened erosion resistance and reduced stability of the rock mass laid a foundation for the large-scale instability of the marginal slope. Under this condition, the eastern flank of the Wushengong Ridge is prone to have slope failures, and it is ascertained by a deposit body of limestone boulders and gravels overlying the limestone bedrock (**Figure 11A**).

In 624 AD, a strong earthquake caused the entire eastern slope of the Wushengong Ridge to collapse, including the above deposit body and a hill north of the ridge. This earthquake caused an over 2 km long slope collapse with a total volume exceeding $7 \times 10^6 \text{ m}^3$ failing. The boulders spread from the frontal edge of the source area to the east bank of the Jinsha River, with a maximum horizontal distance of 550 m. Most of the boulders fell into the Jinsha River, and a small amount of them lie on both banks of the river in a limited range. At the point where the Jinsha River narrowed, a large number of boulders blocked the river, forming a dam and a temporary lake. In a relatively still water environment, a set of lacustrine sand was preserved in a limited area (**Figure 11B**).

The dammed lake had not existed long from the evidence of the thin lacustrine sand layer (10–35 cm thick). As researched previously, landslide dammed lakes may last from several

TABLE 5 | Parameters of earthquakes with intensity \geq IX from Xichang to Dongchuan.

No	Date	Magnitude	Macroscopic epicenter	Epicentral intensity	Epicentral region		Seismogenic fault	Data sources
					(Major axis, minor axis) km	Trend		
1	624/8/18	7.9	Qiaojia	X	(158,33)**	N31°W	Qiaojia Fault	a
2	814/4/6	7	Xichang	IX	—	—	Anninghe Fault	b
3	1489/1/15	6 ³ / ₄	Xichang and Yuexi	IX	(39,18)*	N6°W	Zemuhe Fault	c
4	1732/1/29	6 ³ / ₄	Xichang	IX	(50,21)*	N23°W	Zemuhe Fault	b
5	1733/8/2	7 ³ / ₄	Dongchuan	X	(152,42)*	N11°W	Qiaojia fault and dongchuan Fault	b
6	1850/9/12	7 ¹ / ₂	Xichang-puge	X	(116,29)*	N25°W	Zemuhe Fault	b
7	1966/2/5	6 ¹ / ₂	Dongchuan	IX	(97,53)*	N44°W	Songming Fault	b

Annotation: * from documented data; ** calculated according to the formula (3) in the text; - no data; a. This paper; b. Department of Earthquake Damage Prevention (1995); c. Wen, 2000.

minutes to several thousand years, depending on factors such as volume, size, geometry, sorting of blockage materials, rates of seepage through the blockage, and rates of sediments and water that flow into the newly formed lake (Costa and Schuster, 1988; Peng and Zhang, 2011). Combined with cases in southwest China (Peng and Zhang, 2011), where the longevity of landslide dams is a few hours or more than 10 h, here we suppose several that several hours later, the dam broke and the river reopened its flow (Figure 11C). The boulders in the water were either swept away by the current or settled on the bottom of the riverbed. The remaining boulders even affected the terrain of the riverbed (Figure 4). The boulders on the east bank have experienced a free movement without friction among boulders, which resulted in the boulders having better roundness. With the later influence of artificial reconstruction, the boulders became fewer in number.

Seismic Hazard Assessment of Qiaojia Segment

About 1.3 km NW of the landslide, the floodplain of Heishui River shows a left-lateral displacement of 13 m, which was measured in the field with the laser rangefinder and was considered surface coseismic displacement of one or several earthquakes (Figure 12). Chen and Zhao (1988) found that the Jinsha River and its main tributaries all have more than six terraces. The depositional age of the terraces of the Jinsha River and its first tributaries, such as Nu, Nanpan, Niulan, and Xiao Rivers were obtained (Ji et al., 2000). It is indicated that the T1 terrace of the first tributaries was deposited in 4,500–11,000 years BP, which is later than that of the Jinsha River (9,000–17,000 years BP). The stream trenching rate of the Jinsha River near Qiaojia was also taken into account to constrain the forming age of the Heishui River floodplain. Huang et al. (2010) calculated the stream trenching rate on the Baihetan reach of the Jinsha River for the construction needs of the Baihetan Hydropower station. The results show the average trenching rate is about 1.2 mm/yr since 25 ka, showing an increasing trend since 100 ka. Ding et al. (2017) later took the climate factor into account and gave a 1.17 mm/yr trenching rate since 23.5 ka at Qiaojia. In combination with our field measurement

of the 2 m height of the floodplain, we believe that the lower limit of the age of the floodplain is no earlier than 1700 years BP. As recorded, the earliest earthquake recorded in the Xichang area is the Xichang 111 BC earthquake (Xichang City Chronicle Compilation Committee of Sichuan Province, 1996). In the absence of omissions, there is only one earthquake with a magnitude of $M \geq 6$ since then, that is, the 624 AD earthquake. Apparently, the 624 AD earthquake alone bore the 13 m displacement of the Heishui River floodplain. In addition, it is further confirmed that the macro-epicenter of this earthquake is at this coseismic displacement location. Furthermore, according to the functional relationship between the maximum coseismic displacement and the moment magnitude of Wells and Coppersmith (1994),

$$M_w = 6.81 + 0.78 \cdot \log(MD) \quad (1)$$

Where the MD refers to maximum displacement (m); the moment magnitude of the 624 AD earthquake is calculated to be about 7.7.

Similarly, the functional relationship between the maximum coseismic displacement and the surface wave magnitude of Bonilla et al. (1984),

$$M_s = 7 + 0.78 \cdot \log(MD) \quad (2)$$

Where the MD also refers to maximum displacement (m), giving a result of $M_s 7.9$. As we discussed above, the 624 AD earthquake should have occurred in valley areas south of Xichang, and near Qiaojia. This transforms the Qiaojia area from a historical seismic gap to a potential seismic area.

For the eastern margin of the Tibetan Plateau, $M 6.5$ may represent the magnitude threshold of the surface rupture along the active faults in the region (Xu et al., 2017). Earthquakes with a magnitude less than this threshold generally do not have surface ruptures, and occasionally have secondary surface fractures (Wells and Coppersmith, 1994). Earthquakes with a magnitude greater than or equal to this threshold can form several kilometers to one hundred kilometers of coseismic surface rupture and several meters of coseismic displacement, which directly controls the spatial distribution

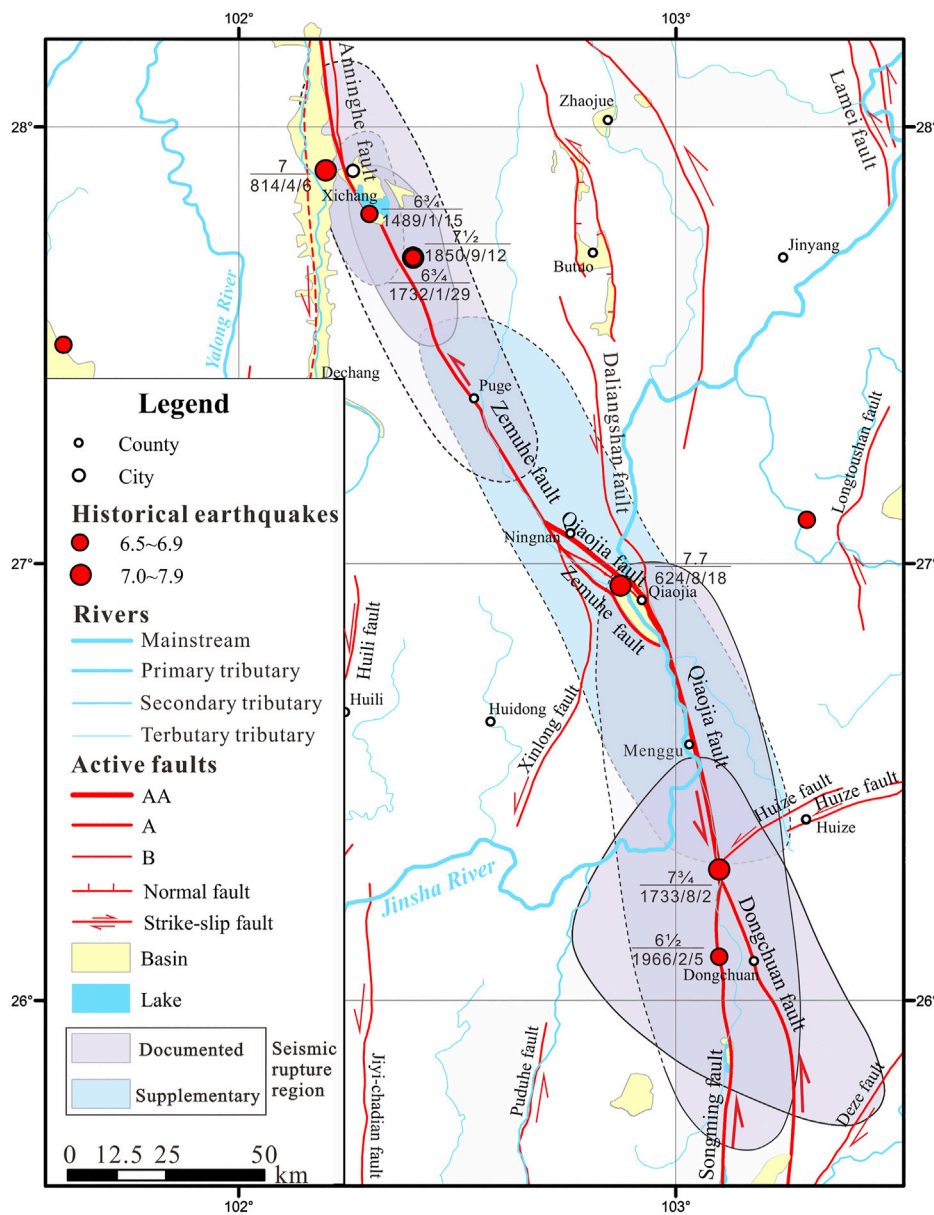


FIGURE 13 | Rupture areas with intensity \geq IX for the historical earthquakes from Xichang to Dongchuan. The dashed circle indicates the area not verified in the field. For the active faults, AA, A, and B indicate their activity of extremely strong, strong, and medium.

of the serious earthquake disaster zone in the Meizoseismal area. Therefore, the distribution of seismic gaps on a fault can be seen directly by statistical analysis of the historical earthquakes with magnitudes ≥ 6.5 and delineation of their rupture areas with intensity \geq IX. Based on this, the authors reorganized the historical earthquakes with intensity \geq IX from Xichang to Dongchuan that involves the Anninghe Fault, the Zemuhe Fault, and the Xiaojiang Fault, from north to south (Table 5). Apart from the 624 AD and 814 AD earthquakes, the rupture areas of other historical earthquakes are all referred to in historical data or previous studies. It should be noted that the

rupture area of the 1489 AD earthquake is the same as the focal area of the $6^{3/4}$ -magnitude earthquake (Wen, 2000), and the VIII area was adopted as the rupture area of the 1952 earthquake. Furthermore, according to the regression of surface rupture length and displacement (Wells and Coppersmith, 1994),

$$\text{Log (SRL)} = 1.49 + 0.64 \cdot \text{log (MD)} \quad (3)$$

The long axis of the rupture area of the 624 AD earthquake was calculated to be 158 km based on the 13 m displacement of the Heishui River floodplain (Figure 13).

No $M \geq 7$ earthquakes have occurred on Qiaojia Segment for the nearly 1,400 years since 624 AD. Such a long elapsed time is close to the average recurrence interval of large earthquakes on the segment around Dongchuan ($1,447 \pm 822$ years) as estimated by Shen et al. (1998). In addition, the late Quaternary strike-slip rate of the Qiaojia Segment is 8.5 ± 1.5 mm/yr, therefore, the strain accumulated since about 1,400 yrs could occur an earthquake with a comparable magnitude. Apparently, the seismic hazard of the Qiaojia area should be considered in the future.

CONCLUSION

Based on the field investigation, the use of high-resolution topographic data, and the OSL and ^{14}C methods, we can conclude:

In 624 AD, a nearly 2 km long failed slope collapse occurred on the west bank of the Qiaojia reach of the Jinsha River, resulting in a temporary dammed lake. This failed slope collapse is suspected to be seismic origin, with several evidences support, including: The landslide is located in the seismic region, its large size with cluster form, the instability of the source area, the limited distribution of landslide mass, and the temporal-coincidence with 624 AD earthquake.

The macro epicenter of the 624 AD earthquake was relocated to Qiaojia, and its magnitude was recalculated to be $M_w 7.7$ or $M_s 7.9$ according to the coseismic displacement of the Heishui River floodplain. Further combining with the rupture regions of other historical earthquakes in the Xichang-Dongchuan area, it is considered that the 624 AD earthquake filled the seismic gap in the Qiaojia area. However, the nearly 1,400 a long-time elapsed time is close to the average recurrence interval of large earthquakes on the Qiaojia Segment. Therefore, the seismic hazard of the Qiaojia area should be considered in the future.

REFERENCES

- Adams, J. (1981). Earthquake-dammed lakes in New Zealand. *Geology* 9, 215–219. doi:10.1130/0091-7613(1981)9<215:elinz>2.0.co;2
- Bolt, A. B., Horn, L. W., Macdonald, A. G., and Scott, F. R. (1977). *Geological hazards*. New York, NY: Springer-Verlag.
- Bonilla, M. G., Mark, R. K., and Lienkaemper, J. J. (1984). Statistical relations among earthquake magnitude, surface rupture length, and surface fault displacement. *Bull. Seismol. Soc. America* 74 (6), 2379–2411.
- Burrows, C. J. (1975). A 500-year-old landslide in the Acheron River valley, Canterbury. *N. Z. J. Geology. Geophys.* 18, 357–360. doi:10.1080/00288306.1975.10418206
- Chen, F. B., and Zhao, Y. T. (1988). *The neotectonics in the panzhuhua-xichang region of China*. Chengdu, China: Sichuan Science and Technology Press.
- Chen, Y., Li, S.-H., Sun, J., and Fu, B. (2013). OSL dating of offset streams across the Altyn Tagh Fault: channel deflection, loess deposition and implication for the slip rate. *Tectonophysics* 594, 182–194. doi:10.1016/j.tecto.2013.04.002
- Cornforth, D. H. (2005). *Landslides in practice: investigation, analysis, and remedial preventative options in soils*. Chichester, United Kingdom: John Wiley & Sons.
- Costa, J. E., and Schuster, R. L. (1988). The formation and failure of natural dams. *Geol. Soc. Am. Bull.* 100, 1054–1068. doi:10.1130/0016-7606(1988)100<1054:tfafon>2.3.co;2
- Crozier, M. J. (1992). "Determination of paleoseismicity from landslide," in *Landslides (Glissement de terrain)*. Editor D. H. Bell (New Zealand: Balkema), 1173–1180. Department of Earthquake Damage Prevention, State Seismological Bureau (1995). *Catalog of strong earthquakes in China (23rd century B.C.-1911 A.D)*. Beijing, China: Seismological Press.

DATA AVAILABILITY STATEMENT

The original contributions presented in the study are included in the article/Supplementary Material, further inquiries can be directed to the corresponding author.

AUTHOR CONTRIBUTIONS

MH designed the study, analyzed the data, and wrote the manuscript; ZW proposed and participated in designing the study, and reviewed the paper; KR participated in designing the study, and reviewed the paper; SA improved and polished the paper; XH and JZ participated in the field investigation. All authors approved the final version of the manuscript.

FUNDING

This research has been funded by the China Geology Survey Projects (Grant Nos. 12120114002101, DD20160268) and the financial grants from the National Natural Scientific Foundation of China (Grant No. U2002211).

ACKNOWLEDGMENTS

The authors are grateful to the editor and three reviewers for their thorough and constructive reviews, which greatly improved the quality of this manuscript. The authors also would like to thank Guanghao Ha for his kind help during the fieldwork. In addition, the first author thanks the China Scholarship Council (CSC) for the scholarship and financial support.

- Ding, Y. Y., Zhang, X. J., He, Z. X., Hu, D. G., and Wang, C. Q. (2017). River incision behavior response to climate change during the last glacial period. *Geoscience* 31 (2), 394–405. (in Chinese with English abstract).
- Evans, S. G., and Clague, J. J. (1994). Recent climatic change and catastrophic geomorphic processes in mountain environments. *Geomorphology* 10, 107–128. doi:10.1016/0169-555x(94)90011-6
- Feng, Z., Wu, Z. H., Cao, J. W., Hu, M. M., Ha, G. H., and Kang, H. X. (2019). Engineering geological characteristics of gigantic pre-historic landslide along Qiaojia section of the Xiaojiang fault. *Acta Geosci. Sin.* 40 (4), 629–636. doi:10.3975/cagsb.2019.012401 (in Chinese with English abstract).
- Highland, L. M., and Bobrowsky, P. (2008). *The landslide handbook—a guide to understanding landslides*, Reston, Virginia: U.S. Geological Survey Circular. 129.
- Huang, D., Yang, D. Y., Lu, F., Li, L. P., Ge, Z. S., Shi, A. C., et al. (2010). Incision rates of the baihetan section of the Jinsha River. *Quat. Sci.* 30 (5), 872–876. (in Chinese with English abstract).
- Ji, F. J., Zheng, R. Z., Li, J. P., and Yin, J. H. (2000). Chronological research of geomorphic surface of lower terraces along several major rivers in the east and west of Yunnan province. *Seismol. Geology.* 22 (3), 265–276. (in Chinese with English abstract).
- Jibson, R. W. (1996). Use of landslides for paleoseismic analysis. *Eng. Geol.* 43, 291–323. doi:10.1016/s0013-7952(96)00039-7
- Jibson, W. R. (2015). "Paleoseismology and landslides," in *Encyclopedia of earthquake engineering*. Editors M. Beer, I. A. Kougioumtzoglou, E. Patelli, and S. K. Au (Heidelberg: Springer).
- Jibson, W. R. (2009). "Using landslides for paleoseismic analysis," in *Paleoseismology*. Editor P. J. McCalpin (Cambridge, MA: Academic Press), 565–601.

- Johnson, K., Nissen, E., Saripalli, S., Arrowsmith, J. R., McGarey, P., Scharer, K., et al. (2014). Rapid mapping of ultrafine fault zone topography with structure from motion. *Geosphere* 10 (5), 969–986. doi:10.1130/ges01017.1
- Keefer, D. K. (1984). Landslides caused by earthquakes. *Geol. Soc. America Bull.* 95, 406–421. doi:10.1130/0016-7606(1984)95<406:lcb>2.0.co;2
- Keefer, D. K. (1994). The importance of earthquake-induced landslides to long-term slope erosion and slope-failure hazards in seismically active regions. *Geomorphology* 10, 265–284. doi:10.1016/0169-555x(94)90021-3
- Li, T.-T., Pei, X.-J., Huang, R.-Q., and Jin, L.-D. (2016). The formation and evolution of the Qiaojia pull-Apart Basin, north Xiaojiang fault zone, southwest China. *J. Mt. Sci.* 13, 1096–1106. doi:10.1007/s11629-015-3778-1 (in Chinese with English abstract).
- Liu, J., Zeng, L. S., Ding, L., Taponnier, P., Gaudemer, Y., Wen, L., et al. (2009). Tectonic geomorphology, active tectonics and lower crustal channel flow hypothesis of the southeastern Tibetan Plateau. *Chin. J. Geology.* 44 (4), 1227–1255. (in Chinese with English abstract).
- Lou, B. T. (1996). *A comprehensive complication of historic and recent earthquakes disaster status in China*. Beijing, China: Seismological Press.
- Lucier, A., Jong, S. M. D., and Turner, D. (2014). Mapping landslide displacements using structure from motion (SfM) and image correlation of multi-temporal UAV photography. *Prog. Phys. Geogr. Earth Environ.* 38 (1), 97–116. doi:10.1177/0309133313515293
- Massey, C., Townsend, D., Rathje, E., Allstadt, K. E., Lukovic, B., Kaneko, Y., et al. (2018). Landslides triggered by the 14 november 2016 Mw 7.8 Kaikōura earthquake, New Zealand. *Bull. Seismol. Soc. America* 108 (3B), 1630–1648. doi:10.1785/0120170305
- McCalpin, P. J. (2009). “Application of paleoseismic data to seismic hazard assessment and neotectonic research,” in *Paleoseismology*. Editor P. J. McCalpin (Cambridge, MA: Academic Press), 1–106.
- Meunier, P., Hovius, N., and Haines, A. J. (2007). Regional patterns of earthquake-triggered landslides and their relation to ground motion. *Geophys. Res. Lett.* 34, L20408. doi:10.1029/2007GL031337
- Nikonov, A. A. (1988). Reconstruction of the main parameters of old large earthquakes in Soviet Central Asia using the paleoseismogeological method. *Tectonophysics* 147, 297–312. doi:10.1016/0040-1951(88)90191-6
- Pánek, T. (2015). Recent progress in landslide dating. *Prog. Phys. Geogr. Earth Environ.* 39 (2), 168–198. doi:10.1177/0309133314550671
- Parkash, S. (2012). *Training module on comprehensive landslides risk management*. New Delhi, India: National Institute of Disaster Management, 282
- Peng, M., and Zhang, L. M. (2011). Breaching parameters of landslide dams. *Landslides* 9 (1), 13–31. doi:10.1007/s10346-011-0271-y
- Perrin, N. D., and Hancox, G. T. (1992). “Landslide-dammed lakes in New Zealand - preliminary studies on their distribution, causes and effects,” in *Landslides (Glissements de terrain)*. Editor D. H. Bell (New Zealand: Balkema), 1457–1466.
- Shen, J., Wang, Y. P., Song, F. M., and Li, Y. Z. (1998). Relative creep rate and characteristic earthquake recurrence interval—an example from the Xiaojiang Fault Zone in Yunnan, China. *Seismol. Geology.* 20 (4), 328–331. (in Chinese with English abstract).
- Snavely, N., Seitz, S. M., and Szeliski, R. (2008). Modeling the world from internet photo collections. *Int. J. Comput. Vis.* 80 (2), 189–210. doi:10.1007/s11263-007-0107-3
- Solonenko, V. P. (1977). Landslides and collapses in seismic zones and their prediction. *Bull. Int. Assoc. Eng. Geol.* 15, 4–8. doi:10.1007/bf02592633
- Song, X. B., Shi, A. C., Zheng, W. F., and Jin, R. X. (2012). Analysis of slope deformation characteristics and mechanism in left bank of Baihetan Hydropower Station Jinsha River. *Chin. J. Rock Mech. Eng.* 31 (S2), 3533–3538. (in Chinese with English abstract).
- Stewart, J., and Wren, J. (2005). “Geotechnical aspects,” in *Consortium of Universities for Research in Earthquake Engineering (CUREE), Engineering guidelines for the assessment and repair of earthquake damage in residential wood frame buildings (USA: CUREE Publication)*. No. EDA-06 Version 2005-4.
- Tibaldi, A., Ferrari, L., and Pasquaré, G. (1995). Landslides triggered by earthquakes and their relations with faults and mountain slope geometry: an example from Ecuador. *Geomorphology* 11, 215–226. doi:10.1016/0169-555x(94)00060-5
- Varnes, D. J. (1978). “Slope movement types and processes,” in *Landslides, analysis and control, transportation research board, special report no. 176*. Editors R. L. Schuster and R. J. Krizek (Washington DC: National Academy of Sciences), 11–33.
- Wang, Z. H. (1996). Remote sensing investigation for a huge landslide—Qiaojia county landslide. *Remote sensing Environ. China* 11 (4), 280–284. (in Chinese with English abstract).
- Wei, W. X., Jiang, Z. S., Wu, Y. Q., Liu, X. X., Zhao, J., Li, Q., et al. (2012). Study on motion characteristics and strain accumulation of the Xiaojiang Fault Zone. *J. Geodesy Geodynamics* 32 (2), 11–15. (in Chinese with English abstract).
- Wells, D. L., and Coppersmith, K. J. (1994). New empirical relationships among magnitude, rupture length, rupture width, rupture area, and surface displacement. *Bull. Seismol. Soc. America* 84 (4), 974–1002.
- Wen, X., Du, F., Long, F., Fan, J., and Zhu, H. (2011). Tectonic dynamics and correlation of major earthquake sequences of the Xiaojiang and Qujiang-Shiping fault systems, Yunnan, China. *Sci. China Earth Sci.* 54 (10), 1563–1575. doi:10.1007/s11430-011-4231-0
- Wen, X. Z. (2000). The character of rupture segmentation of the Xianshuihe-Anninghe-Zemuhe Fault Zone, western Sichuan. *Seismol. Geology.* 22 (3), 239–249. (in Chinese with English abstract).
- Westoby, M. J., Brasington, J., Glasser, N. F., Hambrey, M. J., and Reynolds, J. M. (2012). ‘Structure-from-Motion’ photogrammetry: a low-cost, effective tool for geoscience applications. *Geomorphology* 179, 300–314. doi:10.1016/j.geomorph.2012.08.021
- Wu, Z. H., and Zhou, C. J. (2018). *Distribution map of active faults in China and its adjacent seas (1:5,000,000) and its specification*. Beijing, China: Geological Publishing House.
- Xichang City Chronicle Compilation Committee of Sichuan Province (1996). *Xichang chronicles*. Chengdu, China: Sichuan Renmin Press.
- Xu, X. W., Wu, X. Y., Yu, G. H., Tan, X. B., and Li, K. (2017). Seismo-Geological signatures for identifying $M \geq 7.0$ earthquake risk area and their preliminary application in mainland China. *Seismol. Geology.* 39 (2), 219–275. (in Chinese with English abstract).
- Xu, Z. M., Zhao, W. L., and Huang, R. Q. (2011). Engineering geological characteristics of Zhaizicun giant ancient landslide along Jinsha River and its occurrence mechanisms. *Chin. J. Rock Mech. Eng.* (S2), 3539–3550. (in Chinese with English abstract).
- Zeng, Q. L., Yuan, G. X., McSaveney, M., Ma, F. S., Wei, R. Q., Liao, L. Y., et al. (2020). Timing and seismic origin of Nixu rock avalanche in southern Tibet and its implications on Nimu active fault. *Eng. Geology.* 268, 1–14. doi:10.1016/j.enggeo.2020.105522
- Zhang, J. M., Xu, Z. M., Li, Q. K., Zhang, W. F., and Fu, B. (2012). New findings of ancient landslide and geological tectonics constraints along the Jinsha River near Zhaizicun, Yongsheng, Yunnan, China. *J. Jinlin Univ. (Earth Sci. Edition)* 42 (S3), 206–213. (in Chinese with English abstract).
- Zhang, K. Q., Wu, Z. H., Lv, T. Y., and Feng, H. (2015). Review and progress of OSL dating. *Geol. Bull. China* 34 (1), 183–203. (in Chinese with English abstract).
- Zhang, X., Wang, Y. S., and Liang, R. F. (2018). Assessment of landslide hazard in the middle and northern Xiaojiang Fault Zone based on GIS. *Geology. Exploration* 54 (3), 623–633. (in Chinese with English abstract).
- Zhang, Y. S., Guo, C. B., and Zhou, N. J. (2013). Characteristics of Chongjianghe landslide at a branch of Jinsha River and its local reactivation mechanism. *Chin. J. Geotechnical Eng.* 35 (3), 445–453. (in Chinese with English abstract).
- Zhao, C., Kang, Y., Zhang, Q., Lu, Z., and Li, B. (2018). Landslide identification and monitoring along the Jinsha River catchment (Wudongde reservoir area), China, using the InSAR method. *Rem. Sens.* 10, 1–20. doi:10.3390/rs10070993
- Zhao, J., Jiang, Z. S., Niu, A. F., Liu, J., Wu, Y. Q., Wei, W. X., et al. (2015). Study on dynamic characteristics of fault locking and fault slip deficit in the eastern boundary of the Sichuan-Yunnan rhombic block. *Chin. J. Geophys.* 58 (3), 872–885. (in Chinese with English abstract).

Conflict of Interest: The authors declare that the research was conducted in the absence of any commercial or financial relationships that could be construed as a potential conflict of interest.

Copyright © 2021 Hu, Wu, Reicherter, Ali, Huang and Zuo. This is an open-access article distributed under the terms of the Creative Commons Attribution License (CC BY). The use, distribution or reproduction in other forums is permitted, provided the original author(s) and the copyright owner(s) are credited and that the original publication in this journal is cited, in accordance with accepted academic practice. No use, distribution or reproduction is permitted which does not comply with these terms.